Geophysical Journal International

Geophys. J. Int. (2018) **213,** 2138–2146
Advance Access publication 2018 March 15
GJI Seismology

doi: 10.1093/gji/ggy098

Imaging the Variscan suture at the KTB deep drilling site, Germany

Irene Bianchi and Götz Bokelmann

Institut für Meteorologie und Geophysik, Universität Wien, 1090 *Vienna, Austria. E-mail:* *irene.bianchi@univie.ac.at*

Accepted 2018 March 14. Received 2018 March 2; in original form 2017 October 2

SUMMARY

The upper crust of the KTB (Kontinentales Tiefbohrprogramm) area in the Southeastern Germany is a focal point for the Earth Science community due to the huge amount of information collected throughout the last 30 yr. In this study, we explore the crustal structure of the KTB area through the application of the Receiver Function (RF) technique to a new data set recorded by nine temporary seismic stations and one permanent station. We aim to unravel the isotropic structure and compare our results with previous information from the reflection profiles collected during the initial site investigations. Due to the large amount of information collected by previous studies, in terms of *P*-wave velocity, depth and location of major reflectors, depth reconstruction of major faults zones, this area represents a unique occasion to test the resolution capability of a passive seismological study performed by the application of the RF. We aim to verify which contribution could be given by the application of the RF technique, for future studies, in order to get clear images of the deep structure and up to which resolution. The RF technique has apparently not been applied in the area before, yet it may give useful additional insight in subsurface structure, particularly at depths larger than the maximum depth reached by drilling, but also on structures in the upper crust, around the area that has been studied in detail previously. In our results v_S-depth profiles for stations located on the same geological units display common features and show shallow *S*-wave velocities typical of the outcropping geological units (i.e. sedimentary basin, granites and metamorphic rocks). At around 10 km depth, we observe a strong velocity increase beneath all stations. For the stations located in the centre of the area, this variation is weaker, which we assume to be the signature of the main tectonic suture in the area (i.e. the Saxothuringian-Moldanubian suture), along a west-to-east extended region, may be due to the presence of the allochthonous klippe trapped between the main crustal terrains that came in touch during the Variscan orogeny. In the lower crust we see only small variations throughout the area, at the resolution that is possible with a small temporary experiment with just 10 stations.

Key words: Composition and structure of the continental crust; Structure of the Earth; Europe; Body waves; Crustal imaging; Crustal structure.

1 INTRODUCTION

The Continental Deep Drilling Project, or ‘Kontinentales Tiefbohrprogramm der Bundesrepublik Deutschland’, well-known under its abbreviation ‘KTB’, has been one of the most ambitious geoscience projects and one of the largest in Germany and Europe till now. During the exploration phase that took place in the eighties and nineties, crustal rocks have been drilled down to 9 km depth. The project profited from earlier seismic reflection profiles that were recorded in the context of the German Continental Seismic Reflection Program (DEKORP), with the aim of combining together direct and indirect information on the crustal structure of the area. The KTB drilling site is located on the Variscan belt of Europe, formed after several tectonic episodes from Early Palaeozoic rifting within the basement of Gondwana, to the Late Ordovician closure through plate convergence (Franke 1989). The central European crust, after being subject to several reactivations, is relatively thin (25–30 km) and extremely heterogeneous both laterally and vertically with high and low velocity layers at different depths, penetrative deformations and presence of intrusions from late-Variscan granites (Emmermann 1989).

During the intense site investigations, large amounts of geological and geophysical data were collected. Their joint interpretation together with the results from the borehole measurements provides an integrated view of the geology near the drilling site (Haak & Jones 1997). The area surrounding the drilling site is called the ‘Zone of Erbendorf-Vohenstrauß’ (ZEV; Fig. 1). It is situated at the western border of the outcrop of the Variscan Belt and has been

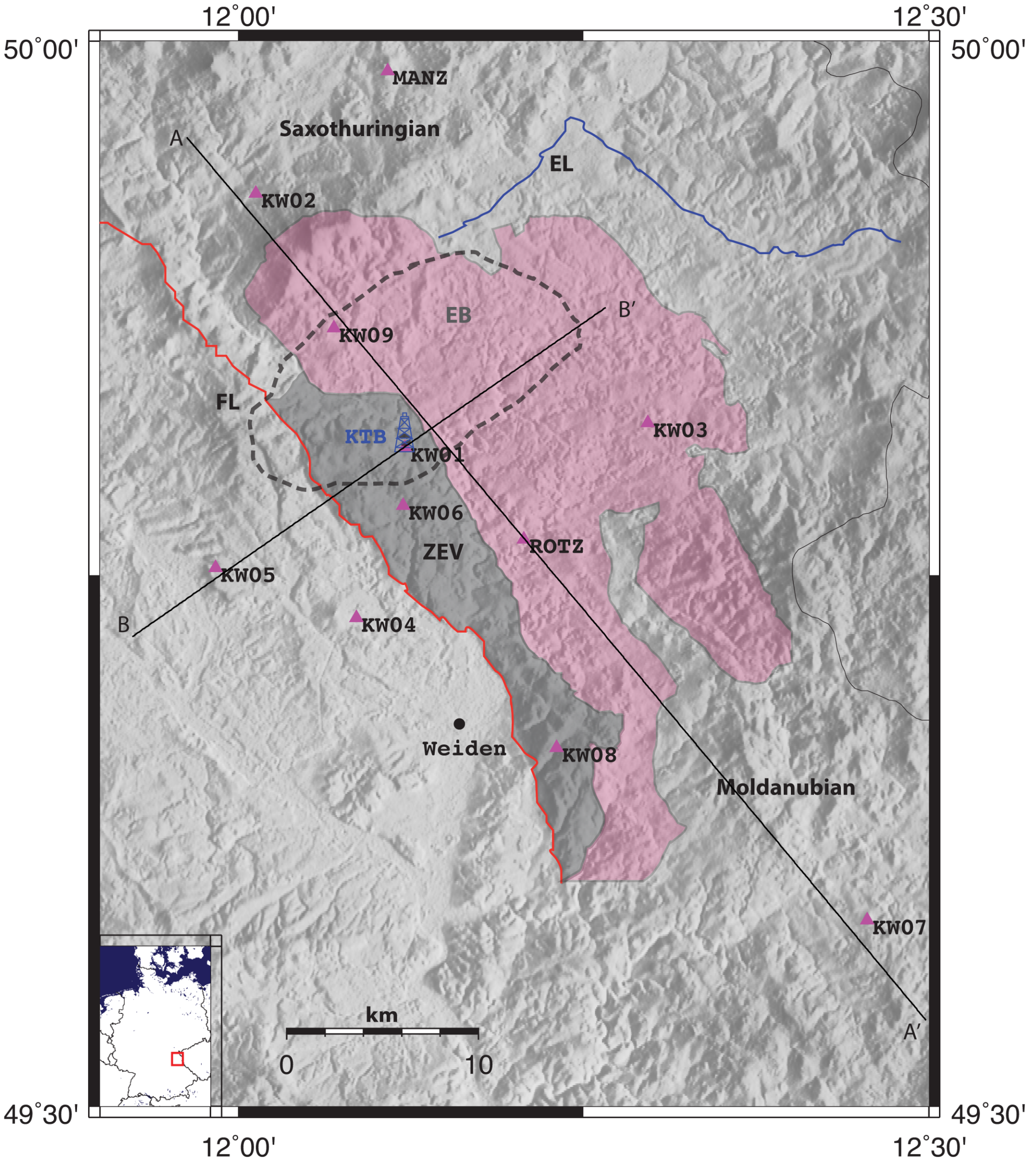

Figure 1. Map of the study area showing the location of the seismic stations (purple triangles) and of the KTB deep drilling site. Grey shades show the areal extension of the Zone of Erbendorf Vohenstrauss (ZEV). The grey dashed line is a surface projection of the buried Erbendorf Body (EB). The pink shaded area shows the extension of the Falkenberg granites. FL, Franconian Lineament; EL, Ebreichsdorf Lineament. The lines represent the traces of the profiles shown in Fig.5.

proposed to be an allochthonous klippe transported to its current location from the South. The Franconian Lineament (FL) is a fault zone less than 10 km from the KTB site, separating the crystalline metabasites and gneisses of the ZEV from younger Mesozoic sediments. It is believed to be associated with late Variscan (early Triassic and Cretaceous) reactivation of an older strike-slip fault as a reverse thrust, resulting from a changed direction of stress (SW–NE compression, see Wagner *et al.* 1997). We selected the KTB area to perform a passive seismological experiment; nine broad-band three-component seismic stations have been deployed and recorded for 2 yr (see Bianchi *et al.* 2015 for the description of the experiment), in order to collect teleseismic earthquakes for the computation of *P* receiver functions (RFs). The aim of the project was to verify to which degree it is possible to infer the crustal structures of the KTB and greater area, whether the RF analysis might reinforce previous knowledge of the subsurface structures, or it might help unravel different or new aspects not yet discovered by previous investigations. We infer *S*-wave depth-velocity variations at each station and interpolate along two profiles coinciding with two of the previous active-seismic profiles acquired in the area during the DEKORP experiment. Similarities and differences between our and previous results give an idea of the potential of the RF technique, its resolution power and how far it can be exploited in order to give images of the fine layered structure, even in an area holding steeply dipping features.

With this study, we model the v_S velocities from the top to the bottom of the crust in an area of complex and high 3-D geology, with occurrence of several strike-slip and high-angle normal faults, vertical and horizontal tension gashes and intrusions (Wagner *et al.* 1997). The RF technique, although non-unique, is a good passive methodology applicable in the area to retrieve velocity models of the crust, in places where high lateral resolution is required. Local

Earthquake Tomography (LET) would be a powerful tool as well, but it requires a high number of local events in order to sample the region, which is not the case of southern Germany, where the seismicity is low. During the 2 yr of recording time of our stations, six events with $M \geq 2$ occurred within the study area, moreover the depth of such events has been estimated to be above 10 km, that means, that it would not be possible to provide images (through LET) of the crust beneath 10 km depth. On the other hand, many teleseismic traces have been recorded by our stations, but teleseismic tomography would not give high definition images of the crust; it is rather employed for imaging the mantle (e.g. Nolet 1987).

2 TECTONIC SETTING OF THE STUDY AREA

The region hosting the deployed seismic stations has been focus of several geophysical investigations during the nineties (DEKORP Research Group 1987; DEKORP Research Group 1988; Eisbacher *et al.* 1989; Lüschen *et al.* 1996; Harjes *et al.* 1997; DEKORP and Orogenic processes Working Groups 1999; Muller *et al.* 1999). Fig. 1 shows the major surface geological units as well as main tectonic lines around the drilling site. The deep borehole was placed into the gneiss rocks of the ZEV. The ZEV is bordered by the FL on the west and by the Falkenberg granites to the east; granites subsurface shape and extent, as well as information on their emplacement and intrusional tectonic settings remain poorly understood (Trzebski *et al.* 1997).

Two main crustal terrains constitute the geology of the area, namely the Saxothuringian (in the NW of the area) and Moldanubian (in the SE of the area). These two terrains came in contact during the Variscan orogenesis and their suture line is supposed to lie in the study area, hidden by the ZEV and granites on the east and by the sedimentary layers on the west. The Saxothuringian consists of Precambrian and Cambrian metasediments, while the Moldanubian is represented by monotonous paragneiss and micaschists; the grade of metamorphism and schistosity of the latter is much stronger than in the Saxothuringian. The ZEV is a pile of metamorphic (high- and low-grade) rocks, showing alternance between paragneiss and amphibolites, extremely folded and faulted by a fault-system related to the outcropping FL.

The ZEV metamorphic body has been drilled for the whole depth extension of the KTB drill, betraying the expectations of reaching the Saxothuringian-Moldanubian boundary below few kilometres of metamorphic rocks.

Seismic studies have pointed out the presence of a structural element at depth called 'Erbendorf body'; this has been imaged as a highly reflective structure that is associated with high velocities. It is located in the middle crust (between 8 and 12 km depth) below the drill site (Hirschmann 1996), probably representing the roots of the ZEV.

3 DATA

We selected high signal-to-noise (S/N) ratio teleseismic events from epicentral distances (Δ) of 30°–100° and magnitude $M_b > 5.5$ recorded at the nine installed stations and one permanent station. Station ROTZ belongs to the permanent Bayern Network, it is located at the centre of the study area, above the granite unit, just to the east of the Erbendorf body. We analysed the data recorded by ROTZ between 2007 January and 2010 December, obtaining a large data set of very high quality RFs. These RFs display high S/N ratio, clear and pronounced *P*-direct arrival, clear *P*s converted phases that display continuity along the whole backazimuthal sweep and a clear Moho arrival.

The collected teleseismic traces allow covering half of the backazimuthal range (see Fig. 2). The RF data sets were obtained by deconvolution of the vertical from the horizontal recordings into the radial, transverse and vertical coordinate system, where the radial (R) is computed along the great circle path between the epicentre and the station, positive away from the source and the transverse (T) direction is calculated 90° clockwise from R. The deconvolution was performed in the frequency domain (Langston 1979; Ammon 1991), following the approach proposed by Park & Levin (2000), applying a slepian taper to limit the frequency band below about 2 Hz (Langston 1979). The data sets are displayed in Fig. 2 as backazimuthal sweeps. The RFs obtained from the events in Fig. 2 have been binned to increase the S/N ratio. Bins shown in Fig. 2 are obtained by the stacking of RFs for events occurring in the same area. The spatial filter used to define the events that belong to a single bin is 20° wide in backazimuth and 35° wide in Δ, we considered for this analysis the events with epicentral distance between 70° and 100° only, in order to include in the analysis the rays upcoming with a near-vertical incidence angle.

3.1 Data analysis

We show radial and transverse RFs as function of backazimuth in Fig. 2; here various patterns of *P*s conversions can be identified on both R and T. While *P*s delay times and its undulations on the R components mostly refer to the isotropic structure below the seismic station (i.e. isotropic velocity jumps, but differential delay times along the backazimuthal sweep are related to the presence of a dipping interface), reversal of polarizations and occurrence of null directions on the T component identify more complex structure related to inclined interfaces and anisotropy at depth (Levin & Park 1998; Frederiksen & Bostock 2000; Schulte-Pelkum *et al.* 2005; Nagaya *et al.* 2008). The time-derivative character of the transverse phase with respect to the radial component and periodicity of waveform variation over the backazimuth allow the application of a technique for the separation of the backazimuthal harmonics of the R- and T-RFs (radial and transverse RF, respectively) as a function of the incoming wavefield direction (Bianchi *et al.* 2008 and references therein; Bianchi *et al.* 2010). Harmonic decomposition separates the 'isotropic contribution', on the $k = 0$ harmonics and the 'anisotropic/dipping contribution', on the $k = 1, 2$ harmonics. Due to the large amount of information contained in this data set, we discuss and show in this paper the isotropic contribution only and leave the interpretation of the anisotropic/dipping contribution for later studies.

The shear velocity model beneath the stations is investigated by extracting the *a posteriori* probability density function of the v_S at depth, from the $k = 0$ harmonics following the approach developed by Piana Agostinetti & Malinverno (2010). Lateral and vertical resolution of the data depends on the frequency content of the data itself. Here we apply a joint inversion of multiple frequencies RF data (i.e. 0.5, 1, 2 and 4 Hz), where the maximum frequency content controls the degree of resolution in depth. Vertical resolution of RF data has been investigated in details in Piana Agostinetti & Malinverno (2018), where they find that using a maximum cut-off frequency of 4 Hz, the resolution for the depth of a seismic interface within the first 5 km is of about 0.35 km. Given the frequency bands considered, we therefore assume a vertical resolution within

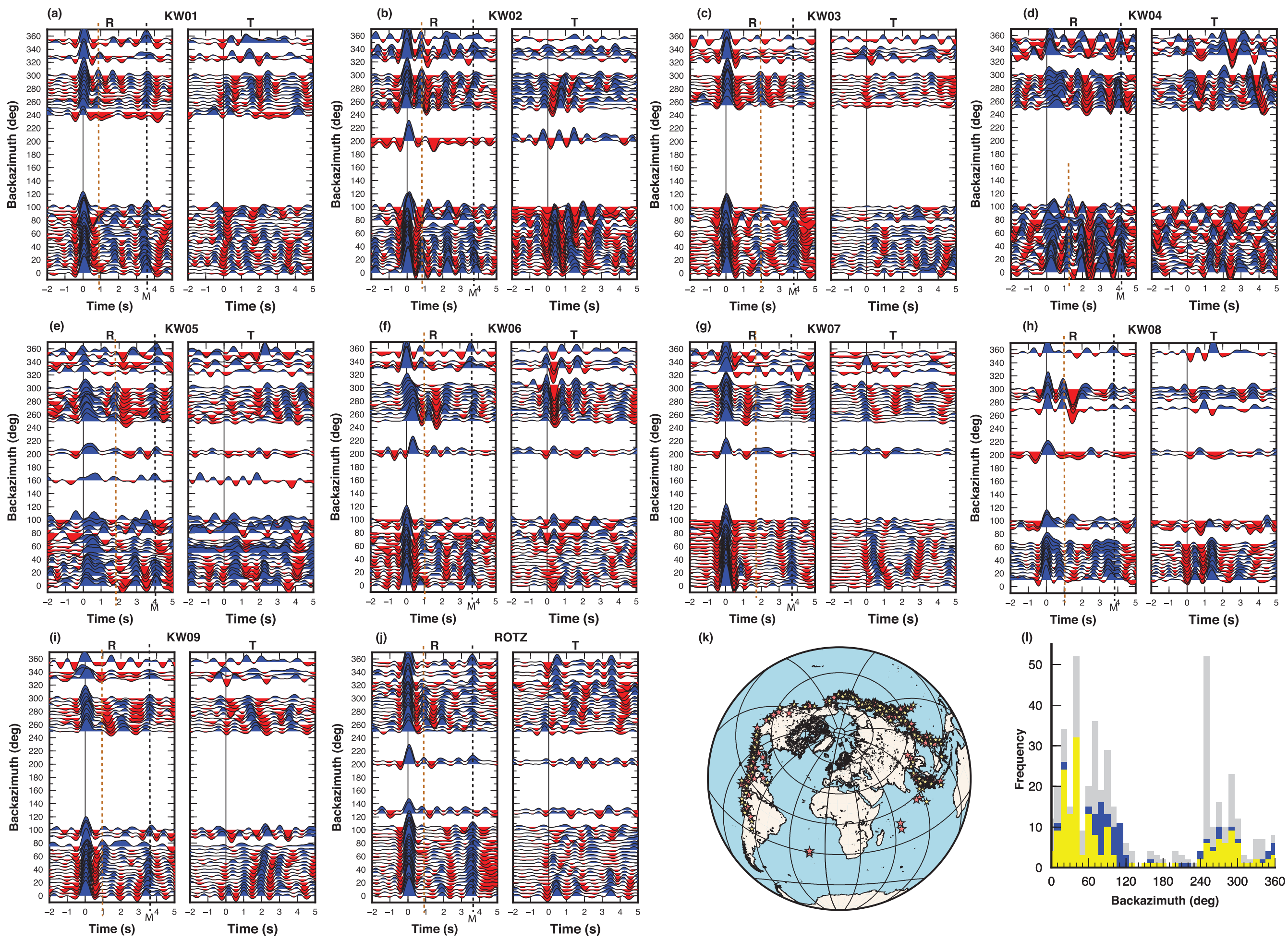

Figure 2. (a-j) Receiver Functions (RFs) for the 10 stations analysed in this work (nine temporary and one permanent); radial (R, left panels) and transverse (T, right panels) RFs are displayed for all stations along backazimuthal sweeps as a function of delay time after the arrival of the direct *P* wave. Blue pulses correspond to positive velocity jumps, while red pulses correspond to negative velocity jumps. Phases associated with an interface at about 10 km depth and with the Moho have been marked respectively by a brown and a black dashed line. (k) Epicentral location of the teleseismic events used for stations ROTZ (red) and KW01 (yellow). (l) Histogram of the number of events recorded for each backazimuthal direction at station KW01, grey for the events recorded, blue for the events selected and yellow for the events used in this study.

0.5 km for the shallowest layers. Lateral resolution is smaller for shallower boundaries and larger for deeper boundaries. Considering horizontal boundaries, the lateral resolution can be assumed to be as large as half of the depth of the retrieved interfaces (Cassidy 1992). Therefore, we can assume a lateral resolution of 5 km for the shallow crust (0–10 km depth).

4 INVERSION METHOD

The Radial Receiver Function (RRF) time-series is used as observed data to constrain the subsurface structure below the seismic station through the solution of the inversion problem. These constraints can be given either as a best-fitting seismic model, or as probability distribution of subsurface parameters. We decide for the second option, due to the fact that a single model generally fails to adequately deal with non-uniqueness of the RRF inverse problem (Ammon *et al.* 1990). Therefore we apply the method presented by Piana Agostinetti & Malinverno (2010), where the v_S parameter space is sampled by a reversible jump Markov chain Monte Carlo (RJMCMC) method in order to retrieve the *a posteriori* probability density of the *S*-wave velocity below a single seismic station. The application of this technique does not require much *a priori* information: both *S*-wave velocity and the number of seismic interfaces at depth are considered as unknowns. As output the posteriori probability distribution (PPD) of the interfaces at depth is obtained. The PPD indicates the number of isotropic layers at depth and their most probable depths (Figs 3b and e). From the PPD, we infer the mean v_S model at depth and its related errors (Figs 3a and d). Bayesian inference does not overcome the non-uniqueness in inverse problems. It simply includes this in the uncertainties in the retrieved parameters. For example, in our case, the Moho depth trades-off with the average velocity in the crust. This fact enlarges the uncertainties in the Moho depth (as shown in Figs 3a and d) and determines the gradual increase of v_S at the Moho. Such a 'gradual Moho' could be an artefact due to our representation and the presence of the trade-off between depth and v_S in the crust and it is related to the nature of the RF signal (i.e. band-limited signal in frequency).

The $k = 0$ harmonics calculated at different frequencies (i.e. 4, 2, 1 and 0.5 Hz, see Figs 3c and f) and their standard deviation are used as observed data. The v_S profiles obtained by the inversion of RF at different cut-off frequencies have been proven to combine the benefits of classical RF inversion (able to resolve v_S discontinuities)

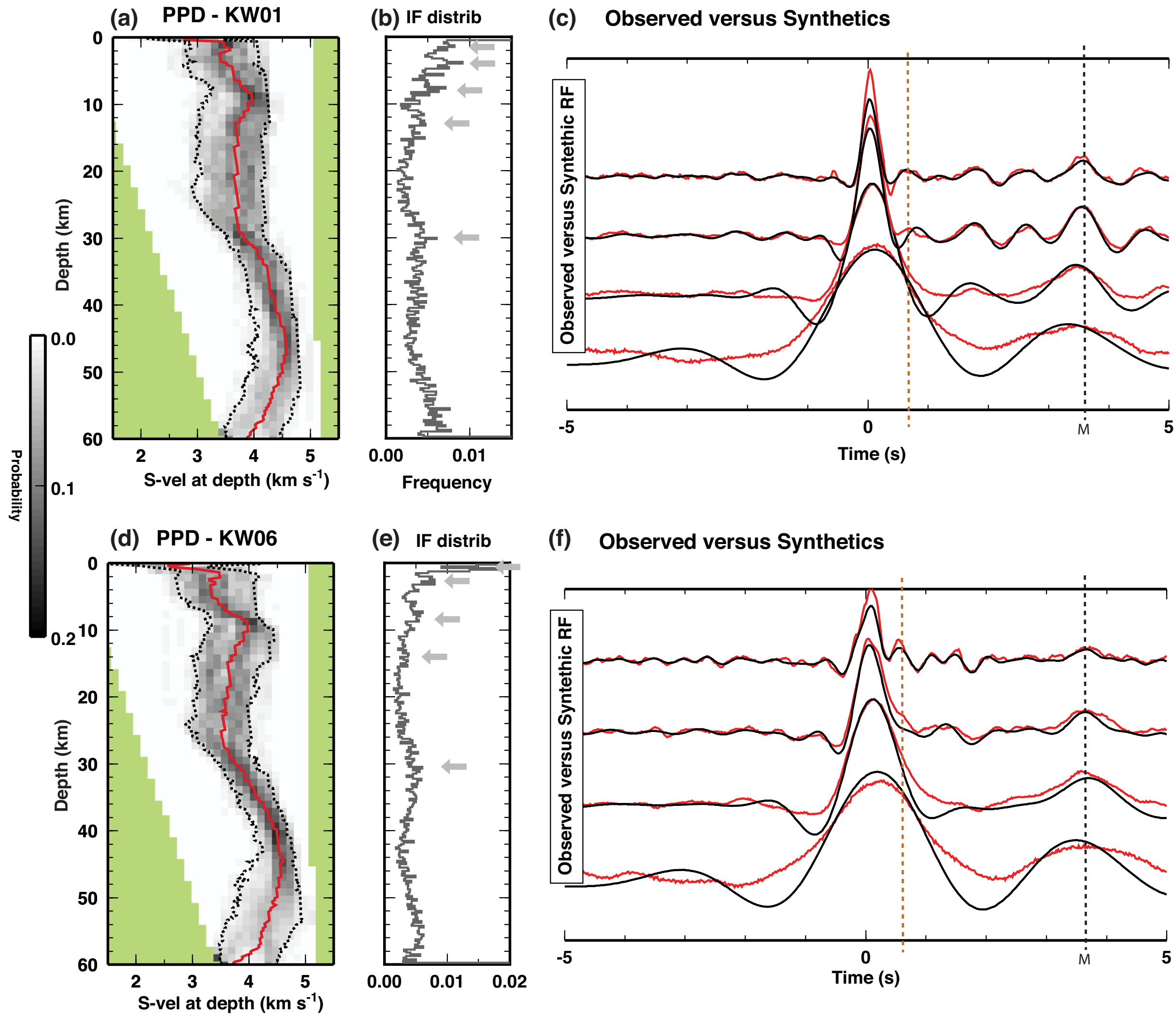

Figure 3. Velocity models for stations KW01 and KW06. (a and d) Posteriori probability distribution (PPD) in depth for v_s and retrieved *S*-velocity model at depth after the application of the RJMCMC; PPD values are shown with grey scale, the red line shows the mean model and the black dotted lines show the 95 per cent posterior confidence interval; (b and e) histogram of interfaces distribution at depth, the arrows highlight the depths at which the probability of encountering an interface is larger; (c and f) observed (black) versus synthetic (red) RF at different frequencies; from top to bottom respectively 4, 2, 1, 0.5 Hz. The phases associated with an interface at about 10 km depth and with the Moho have been marked respectively by a brown and a black dashed line.

and constrain the absolute values of v_S (Svenningsen & Jacobsen 2007; Piana Agostinetti and Malinverno 2018). The PPD of the v_S and v_P/v_S are considered Gaussian and to them is attributed a mean and a standard deviation (σ). For the v_P/v_S, the mean is 1.75 and σ equals 0.05; while they vary with depth for v_S with larger variability for shallower layers. This might be due to a larger variation of lithology. The number of interfaces is considered as unknown itself and varies between 1 and 30; the algorithm is parsimonious, therefore it does not include additional interfaces if not supported by data (Malinverno 2002; Sambridge *et al.* 2006; Piana Agostinetti and Malinverno 2010), it retains the minimum number of interfaces needed for fitting the data, as it can be seen, for example, from Fig. 3(b), the interfaces distribution histogram shows a higher probability of encountering a velocity discontinuity at about 1.5, 4, 8, 13 and 30 km depth for station KW01.

The maximum number of interfaces is given by the resolution of the RF data set. The maximum depth of the interfaces is given by the length of the portion of RF used in the inversion, 0–30 s and it is fixed at 60 km in this study. The misfit between observed and synthetic RF is computed using a classical x^2 function. Between two interfaces, v_S can display a gradient, whereas v_P/v_S is constant. After a burn-in phase of about 25 000 models, which are discarded, the RJMCMC method was set to sample about 175 000 models, from which we computed the PPDs. We ran 95 parallel RJMCMC computations on a linux cluster and obtained an ensemble of about 16×10^6 models.

The RJMCMC search yields two main results: the PPD of the *S* velocity at depth and the distribution of the interface depth sampled during the chain. The PPD at depth, which we show in Figs 3(a) and (d) for stations KW01 and KW06 and in the Supporting Information figures (S1 to S10) for all other stations, is the 1-D marginal distribution of v_S at depth. These distributions do not include information about the correlation of the v_S between different depth levels, which is instead an intrinsic characteristic of the RF itself. Such correlation reduces the variability of the 1-D v_S models sampled from the PPD and the given 95 per cent confidence levels must be interpreted with care. In Piana Agostinetti & Malinverno (2018), this matter has been investigated in detail; there the authors

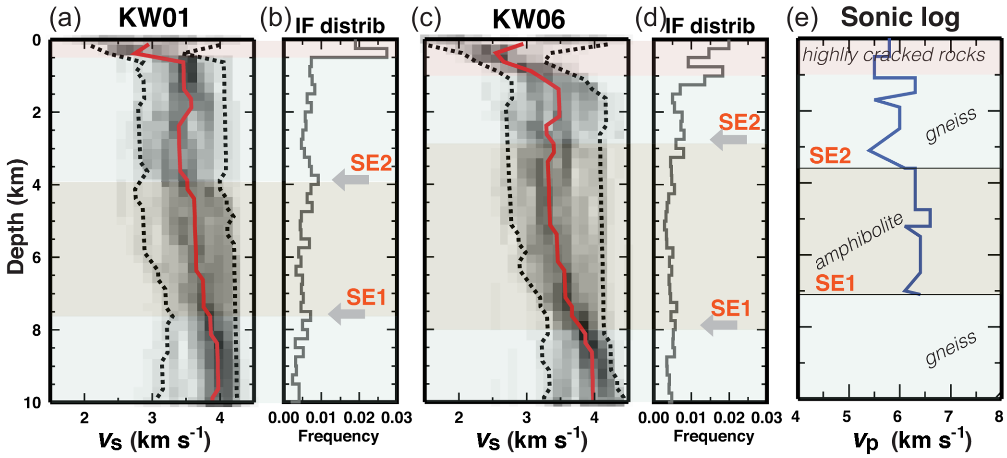

Figure 4. Velocity–depth profiles for the upper 10 km, retrieved at stations KW01 and KW06, compared to v_P from sonic log (Berckhemer *et al.* 1997). Colours on the background highlight the lithological differences at depth. Arrows marked by SE1 and SE2 point at discontinuities that we associate with the two main cataclastic zones encountered during the drilling and associated with the FL fault system.

show that, while 1-D marginal distributions are formally correct, they do not help in visualizing how the RF data constrain the v_S profile at the Moho. In that case, the 95 per cent confidence levels could suggest that a model without the Moho is allowed by the data (i.e. a model with constant velocity between 20 and 40 km depth), but such model is obviously not included in the family of models sampled from the PPD.

5 RESULTS AND DISCUSSIONS

The output of the inversion method we have employed here gives the full PPD as posterior marginal distributions of v_S, interface depths and v_P/v_S as a function of depth. Reminding that this is a conservative representation of the PPD, and does not take into account the correlations between the depth and velocity within the model, and reminding that in any case the multifrequency joint inversion of RF can give good constraints on the upper levels, we are confident in discussing the mean v_s models shown in Fig. 3 and Supporting Information Figs S1–S10, together with the depth distribution of the interfaces [the retrieved PPD of v_S confirms the presence of velocity discontinuities at the depths of model interfaces (Figs 3a, b, d and e)].

We first focus on the upper 10 km of the crust. Stations KW01 and KW06 are located respectively 600 m and 3.5 km from the drill site and the retrieved v_S profiles are compared to the v_P velocity at depth extracted from the sonic log (Berckhemer *et al.* 1997; Fig. 4). The upper 500 m of the profile are characterized by highly cracked rocks, where both *P*- and *S*-waves show low velocities. Then we subdivide the velocity profile into three main units, following the stratification indicated by the lithological profile, where paragneiss prevails in the upper and lower layer, while the middle layer is composed by amphibolite. According to the literature, these three layers are separated by cataclastic zones associated with the fault system of the FL and named respectively SE2 and SE1 (Berckhemer *et al.* 1997). On the velocity profile for station KW01, we highlight velocity jumps at depths corresponding to SE1 and SE2 (3.8 and 7.5 km) associated with a higher frequency of the interface distribution and then identify similar jumps on the velocity profile retrieved for station KW06. Associating the retrieved features to such main discontinuities would not have been possible without the *a priori* knowledge; although we note hints of v_S jumps, it would not be possible to associate it with the cataclastic zones of SE1 and SE2.

Results of the RJMCMC search obtained for stations KW01 and KW06 are displayed in Fig. 3 for the whole crust; results obtained for all other stations are shown in the Supporting Information related to this paper (Figures S1–S10).

According to the similarities of the retrieved velocity models, we can interpret the results by dividing the stations in four groups. The first group is composed of the stations located in the centre of the investigated area, which were installed on top of the metamorphic ZEV. These stations are KW01, KW06 and KW08; we include ROTZ in this group for which the velocity model shows similarities with the others, in particular below the depth of 10 km. We described the upper 10 km of KW01 and KW06 in the previous paragraph; the model for ROTZ shows velocities in the shallow layers of about 3.5 km s^{-1} down to 8 km depth, then a v_S increase up to 3.8 km s^{-1} is noted at about 8 km depth (similar to KW01 and KW06). Although we find 3.5 km s^{-1} for the first 4 km depth at station KW08, this station shows a velocity increase to 4.1 km s^{-1} at about 7 km depth. For all four stations velocities slow down to 3.6 km s^{-1} in the lower crust till reaching the Moho at 30 km depth (32 km below KW08).

The second group is composed of stations KW02 and KW09 that are located at the northern edge of the investigated area. The velocity models for these two stations show differences in the shallower 5 km. For KW09 we show an upper layer with v_s of 3.6 km s^{-1}, dropping to 3.4 km s^{-1} at 4 km depth and increasing up to 4 km s^{-1} at 8 km depth. For station KW02 instead the shallower velocities are higher (i.e. 3.8 km s^{-1}) with a little decrease at about 4 km depth and a fast increase up to 3.9 km s^{-1} at 8 km depth. The lower crust shows velocities on the range of 3.5 km s^{-1} till the Moho located at about 32 km depth.

The third group is composed by the stations KW03 and KW07; the velocity profile obtained for the two stations is similar, but on an average the v_S is higher below station KW07, where it reaches 4 km s^{-1} at 2 and at 10 km depths; while the v_S reaches 3.8 km s^{-1} at the same depths below station KW03. v_S is decreasing in the lower crust to 3.5 km s^{-1} for KW03 and to 3.7 km s^{-1} for KW07. The Moho is at about 31 km depth.

The last group is made of the stations located on the sedimentary basin, west of the FL and consists of stations KW04 and KW05. The velocity models for these two stations display low v_S at the surface

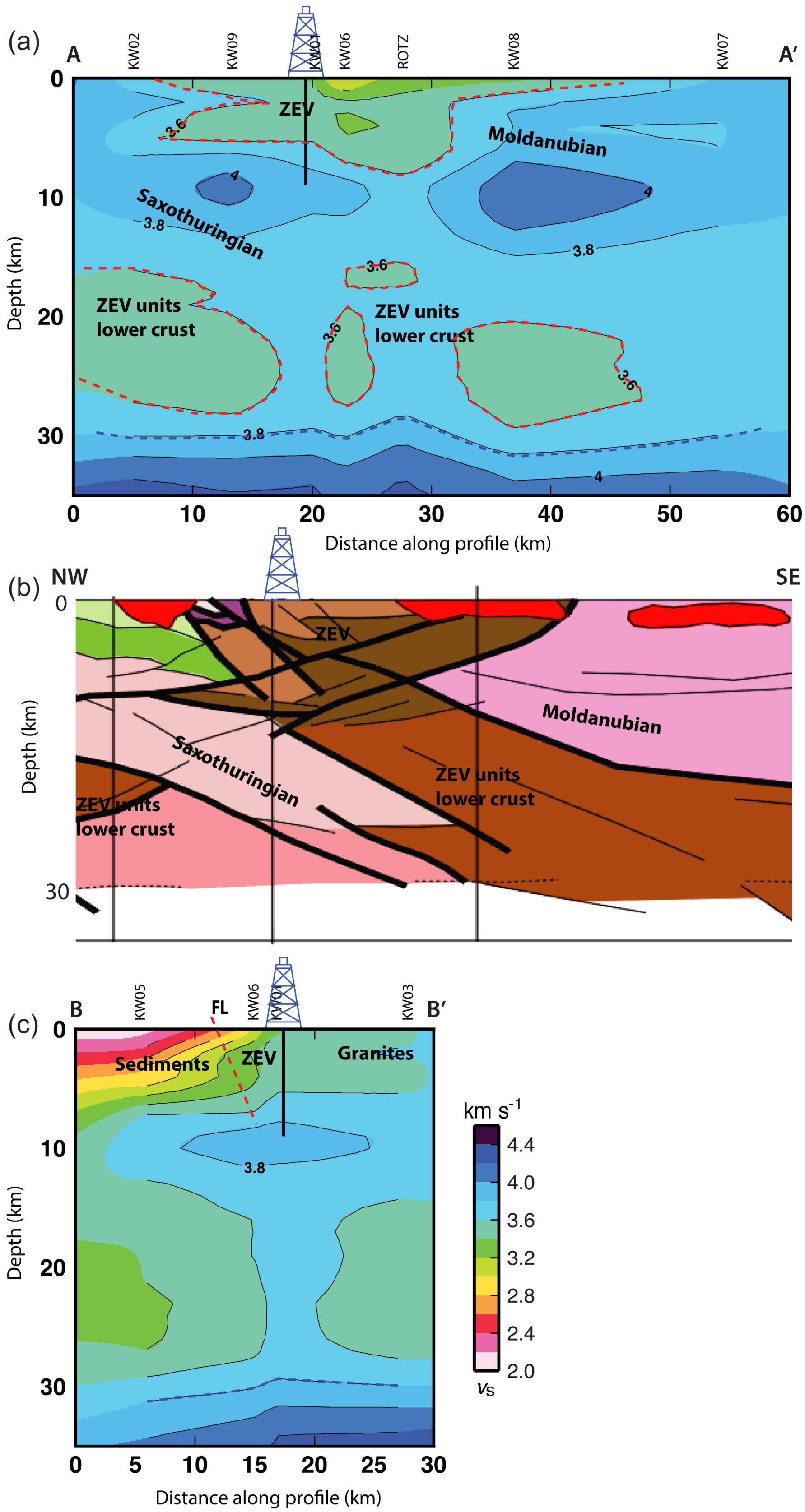

Figure 5. (a) Interpolated *S*-wave velocity along profile AA’ (see Fig. 1 for map trace), the KTB drill site is shown (projected) as reference point. The unit names and red dashed lines are drawn after comparing with the interpreted DEKORP 4 profile (b). (b) Portion of the interpreted DEKORP 4 profile (modified after Hirschmann 1996, credits ICDP, GFZ, Potsdam, Germany), corresponding to the profile in (a). (c) Interpolated *S*-wave velocity along profile BB’ (see Fig. 1 for map trace), the KTB drill site is shown (projected) as reference.

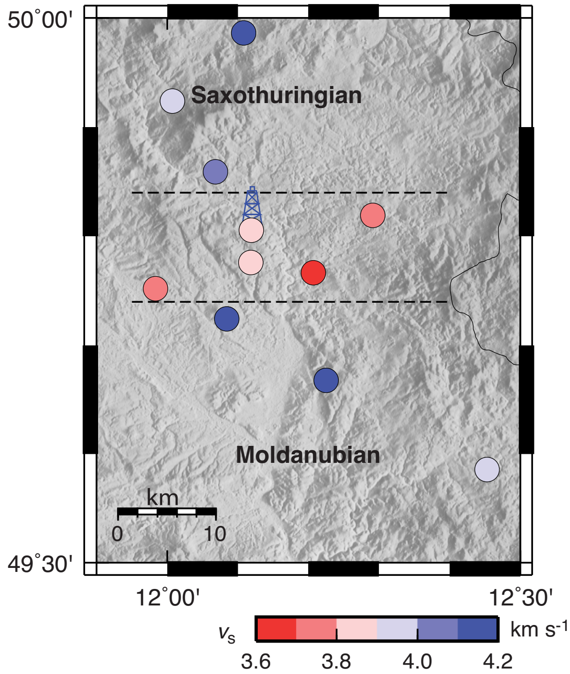

Figure 6. Map of v_s at 10 km depth below each station. Red shades at the station displaying *S*-wave velocities lower than 3.9 km s^{-1} at 10 km depth; blue shades at the station displaying v_s higher than 3.9 km s^{-1} at 10 km. Values below 3.9 km s^{-1} are gathered in the central area of the study region, separating the Saxothuringian to the North from the Moldanubian to the South.

$\sim$2 km s^{-1}, the v_S rapidly increases till 10 km depth but it reaches 4.1 km s^{-1} below station KW04 and reaches 3.7 km s^{-1} at station KW05. The Moho is found at about 30 km depth.

For an interpretation of the results in a broader view, the v_S models have been interpolated along two profiles (Figs 5a and c). The first profile is developed along an NW–SE line and retracing the trend of the DEKORP 4 profile (Hirschmann 1996). The ZEV shows up like a lens that extends from KW09 to KW08, characterized by a v_S of 3.4–3.5 km s^{-1}. It is very thin below KW08 (about 2 km) and it appears at around 4 km depth below the station KW09, at which the granites with higher *S*-velocities (3.7 km s^{-1}) are outcropping.

Outside the ZEV and granite area (i.e. at the location of stations KW02 and KW07) velocities are higher already at shallow depths, reaching 3.9 km s^{-1} at 3 km depth. High velocities occur everywhere down to 12 km depth, with a maximum at 10 km depth. Fig. 6 shows a map with v_s velocities at 10 km depth. The absence of very high velocities for stations KW05, KW06, KW01, KW03 and ROTZ is remarkable: there, v_s reaches values up to around 3.8 km s^{-1}, while v_s is higher elsewhere with values between 3.9 and 4.1 km s^{-1}. The location of these lower velocities at 10 km depth is remarkably oriented on an E–W line and might be related to the presence of the suture zone between the Moldanubian and Saxothuringian tectonic units (or possibly to the upwelling of the granites). Therefore the high velocities at $\sim$10 km in the southern part of the study area might be related to the Moldanubian units, while the high velocities at $\sim$ 10 km on the northern part of the study area might be related to the Saxothuringian units. In the lower crust beneath KW01, KW06 and ROTZ the *S*-velocity slows down to 3.6 km s^{-1} and the same is observed below KW02; this might be related to the presence of the ZEV units in the lower crust, as suggested by the interpretation of the DEKORP 4 profile (Fig. 5b).

In the SW–NE profile (Fig. 5c), we highlight the difference on the two sides of the FL; to the west (KW05) there is a clear feature of the deep sedimentary basin with very low v_s. In the middle of the profile, we encounter the ZEV units with velocities of 3.6 km s^{-1}; further to the east (KW03) the granites are outcropping and we encounter shallow higher velocities as 3.7 km s^{-1}.

The high shear velocities in the middle crust found in all the velocity profiles show an interesting relation with the Erbendorf body that was postulated for the area: a high-velocity feature that also appeared to be associated with high seismic reflectivity. If this is really the same, then the Erbendorf body would be a feature extending over a wider area than just the KTB region and represents perhaps a general feature of the crustal velocity profile. For the narrow region under the KTB, these high seismic velocities were actually less pronounced, which might be due to perturbation by the klippen, or fluid content.

6 CONCLUSION

In this work, we have investigated the (isotropic) characteristics of the crustal structure of the area in the close surroundings of the KTB borehole. With a total of 10 stations, the constraints can only be relatively coarse. Nevertheless, a number of features emerge from the data set that are worth mentioning, for example, the consistency among the velocity models obtained for stations located on similar geological units and the persistent high-velocity anomaly at mid-crustal depth that is related to the occurrence of the Erbendorf body encountered already during active seismic profiling. This high v_S body is interrupted by an area of lower velocity, roughly E–W oriented that might be the expression of the suture of the Variscan orogen that put in contact the two main tectonic units outcropping in the area, that is, Saxothuringian and Moldanubian. Moreover our results from passive imaging highlight the similarities with on-site derived information and, in a comparison with velocities derived from sonic log and lithology changes at depth, show that *S*-wave velocity changes can be associated with the variations in petrophysical characteristics of the rocks.

ACKNOWLEDGEMENTS

We thank Hans Dahlheim, Frank Holzförster and the KTB GEO-Zentrum for providing logistic support during the realization of the field experiment. We thank Wolfgang Rabbel for useful discussions. The KTB-project has been funded by the FWF (Austrian Science Fund), project number P 24218-N24. Credits to ICDP, GFZ, Potsdam, Germany for Fig. 5(b), source of the figure: http://www-icdp.icdp-online.org/sites/ktb/images/Dekorp4.gif. Data are archived at the Institute of Meteorology and Geophysics of the University of Vienna and can be accessed asking directly to IB.

REFERENCES

Ammon, C.J., 1991. The isolation of receiver effects from teleseismic *P* waveforms, *Bull. seism. Soc. Am.,* **81**(6), 2504–2510.

Ammon, C.J., Randall, G.E. & Zandt, G., 1990. On the nonuniqueness of receiver function inversions, *J. geophys. Res.,* **95**(B10), 15 303–15 318.

Berckhemer, H. *et al.*, 1997. Petrophysical properties of the 9-km-deep crustal section at KTB, *J. geophys. Res.,* **102**(B8), 18 337–18 361.

Bianchi, I., Piana Agostinetti, N., De Gori, P. & Chiarabba, C., 2008. Deep structure of the Colli Albani Volcanic District (central Italy) from receiver function analysis, *J. geophys. Res.,* **113**(B9), B09313, doi:10.1029/2007JB005548.

Bianchi, I., Park, J., Piana Agostinetti, N. & Levin, V., 2010. Mapping seismic anisotropy using harmonic decomposition of receiver functions: an application to Northern Apennines, Italy, *J. geophys. Res.,* **115**(B12), B12317, doi:10.1029/2009JB007061.

Bianchi, I., Anselmi, M., Apoloner, M.T., Qorbani, E., Gribovski, K. & Bokelmann, G., 2015. The installation campaign of 9 seismic stations around the KTB site to test anisotropy detection by the Receiver Function Technique, *Adv. Geosci.,* **41,** 11–23.

Cassidy, J., 1992. Numerical experiments in broadband receiver function analysis, *Bull. seism. Soc. Am.,* **82**(3), 1453–1474.

DEKORP and Orogenic processes Working Groups, 1999. Exhumation of subducted crust—the Saxonian granulites from reflection seismic experiment GRANU' 95, *Tectonics,* **18,** 756–773.

DEKORP Research Group, 1987. Near-vertical and wide-angle seismic surveys in the Black Forest, SW Germany, *J. Geophys.,* **62,** 1–30.

DEKORP Research Group, 1988. Results of the DEKORP 4/KTB Oberpfalz deep seismic reflection investigations, *J. Geophys.,* **62,** 69–101.

Eisbacher, G.-H., Lüschen, E. & Wickert, F., 1989. Crustal-scale thrusting and extension in the Hercynian Schwarzwald and Vosges, Central Europe, *Tectonics,* **8**(1), 1–21.

Franke, W., 1989. The geological framework of the KTB drill site, Oberpfalz, in *The German Continental Drilling Program (KTB),* pp. 37–54, eds Emmermann, R. & Wohlenberg, J., Springer-Verlag.

Frederiksen, A.W., & Bostock, M.G., 2000. Modelling teleseismic waves in dipping anisotropic structures, *Geophys. J. Int.,* **141**(2), 401–412.

Emmermann, R., 1989. The KTB pilot hole: tectonic setting, technical data and first results, in *The German Continental Deep Drilling Program (KTB): Site-selection Studies in the Oberpfalz and Schwarzwald,* pp. 527–553, eds Emmermann, R. & Wohlenberg, J., Springer Verlag.

Haak, V. & Jones, A., 1997. Introduction to special section: the KTB deep drill hole, *J. geophys. Res.,* **102**(18), 175–177.

Harjes, H.P. *et al.*, 1997. Origin and nature of crustal reflections: results from integrated seismic measurements at the KTB superdeep drilling site, *J. geophys. Res.,* **102**(B8), 18 267–18 288.

Hirschmann, G., 1996. KTB—the structure of a Variscan terrane boundary: seismic investigation—drilling—models, *Tectonophysics,* **264,** 327–339.

Langston, C.A., 1979. Structure under Mount Rainier, Washington, inferred from teleseismic body waves, *J. geophys. Res.,* **84**(B9), 4749–4762.

Levin, V. & Park, J., 1998. A *P–SH* conversion in layered media with hexagonally symmetric anisotropy: a cookbook, *Pure appl. Geophys.,* **151,** 669–697.

Lüschen, E., Bram, K., Söllner, W. & Sobolev, S., 1996. Nature of seismic reflections and velocities from VSP-experiments and borehole measurements at the KTB deep drilling site in southeast Germany, *Tectonophysics,* **264,** 309–326.

Malinverno, A., 2002. Parsimonious Bayesian Markov chain Monte Carlo inversion in a nonlinear geophysical problem, *Geophys. J. Int.,* **151**(3), 675–688.

Muller, J., Janik, M., & Harjes, H.-P., 1999. The use of wave-field directivity for velocity estimation: moving source profiling (MSP) experiments at KTB, *Pure appl. Geophys.,* **156**(1/2), 303–318.

Nagaya, M., Oda, H., Akazawa, H. & Ishise, M., 2008. Receiver functions of seismic waves in layered anisotropic media: application to the estimate of seismic anisotropy, *Bull. seism. Soc. Am.,* **98**(6), 2990–3006.

Nolet, G., 1987. Seismic wave propagation and seismic tomography, in *Seismic Tomography. Seismology and Exploration Geophysics,* Vol. **5,** ed. Nolet, G., Springer.

Park, J. & & Levin, V., 2000. Receiver functions from multiple-taper spectral correlation estimates, *Bull. seism. Soc. Am,* **90,** 1507–1520.

Piana Agostinetti, N., & Malinverno, A., 2010. Receiver function inversion by trans-dimensional Monte Carlo sampling, *Geophys. J. Int.,* **181,** 858–872.

Piana Agostinetti, N. & Malinverno, A., 2018. Assessing uncertainties in high-resolution, multi-frequency receiver function inversion: a comparison with borehole data, *Geophysics,* **83,** KS11–KS22.

Sambridge, M., Gallagher, K., Jackson, A. & Rickwood, P., 2006. Trans-dimensional inverse problems, model comparison and the evidence, *Geophys. J. Int.,* **167,** 528–542.

Schulte-Pelkum, V., Gaspar, M., Sheehan, A., Pandey, M., Sapkota, S., Bilham, R. & Wu, F., 2005. Imaging the Indian subcontinent beneath the Himalaya, *Nature,* **435,** 1222–1225.

Svenningsen, L., & Jacobsen, B.H., 2007. Absolute *S*-velocity estimation from receiver functions, *Geophys. J. Int.,* **170**(3), 1089–1094.

Trzebski, R., Behr, H.J. & Conrad, W., 1997. Subsurface distribution and tectonic setting of the late-Variscan granites in the northwestern Bohemian Massif, *Geol. Rundsch.*, **86**(Suppl.): S64–S78.

Wagner, G.A. *et al.*, 1997. Post-Variscan thermal and tectonic evolution of the KTB site and its surroundings, *J. geophys. Res.,* **102**(B8), 18 221–18 232.

SUPPORTING INFORMATION

Supplementary data are available at *GJI* online.

Figure S1. Velocity model for station KW01. (a) Posteriori probability distribution (PPD) in depth for v_S and retrieved *S*-velocity model at depth after the application of the RJMCMC; PPD values are shown with grey scale, the red line shows the mean model and the black dotted lines show the 95 per cent posterior confidence interval; (b) same as a), for v_P/v_S; (c) same as (a) zoom at the shallower 10 km; (d) histogram of the isotropic interfaces depth in the seismic structure beneath the station; (e) observed (black) versus synthetic (red) RF at different frequencies; from top to bottom respectively 4, 2, 1, 0.5 Hz; (f) histogram displaying the probability density function of the number of interfaces.

Figure S2. Same as Fig. S1, for station KW06.

Figure S3. Velocity model for station KW02. (a) Posteriori probability distribution (PPD) in depth for v_S and retrieved *S*-velocity model at depth after the application of the RJMCMC; PPD values are shown with grey scale, the red line shows the mean model and the black dotted lines show the 95 per cent *posterior* confidence interval; (b) same as (a), for v_P/v_S; (c) same as (a) zoom at the shallower 10 km; (d) observed (black) versus synthetic (red) RF at different frequencies; from top to bottom respectively 4, 2, 1, 0.5 Hz; (e) histogram of the isotropic interfaces depth in the seismic structure beneath the station.

Figure S4. Same as Fig. S3, for station KW03.

Figure S5. Same as Fig. S3, for station KW04.

Figure S6. Same as Fig. S3, for station KW05.

Figure S7. Same as Fig. S3, for station KW07.

Figure S8. Same as Fig. S3, for station KW08.

Figure S9. Same as Fig. S3, for station KW09.

Figure S10. Same as Fig. S3, for station ROTZ.

Please note: Oxford University Press is not responsible for the content or functionality of any supporting materials supplied by the authors. Any queries (other than missing material) should be directed to the corresponding author for the paper.